

# On Bars, Haloes, their Interaction and their Orbital Structure

E. ATHANASSOULA

*Observatoire de Marseille Provence*

*2, Place Le Verrier*

*13248 Marseille Cédex 04*

*France*

*email: lia@oamp.fr*

**Abstract :** A live halo plays an active role in the formation and evolution of bars by participating in the angular momentum redistribution which drives the dynamical evolution. Angular momentum is emitted mainly by near-resonant material in the bar region and is absorbed mainly by near-resonant material in the halo and in the outer disc. This exchange determines the strength of the bar, the decrease of its pattern speed, as well as its morphology. Thus, contrary to previous beliefs, a halo can help the bar grow, so that bars growing in galaxies with responsive massive haloes can become stronger than bars growing in disc dominated galaxies. During the evolution the halo does not stay axisymmetric. It forms a bar which is shorter and fatter than the disc bar and stays so all through the simulation, although its length grows considerably with time. I discuss the orbital structure in the disc and the halo and compare it with periodic orbits in analytical barred galaxy potentials. A central mass concentration (e.g. a central black hole, or a central disc) weakens a bar and increases its pattern speed. The effect of the central mass concentration depends strongly on the model, being less strong in models with a massive concentrated halo and a strong bar.

**Keywords :** **barred galaxies, dynamical evolution, resonances, bar, halo, peanuts, bulges, orbits, periodic orbits, chaos**

## 1 Introduction

Bars are elongated structures seen in the central parts of a large fraction of disc galaxies. Their morphological, photometrical and kinematical properties have been widely studied. Unfortunately, there is no review of observational results which is both complete and up

to date, but the reader can consult Kormendy (1982); Bosma (1992); Buta, Crocker & Elmegreen (1996); Athanassoula, Bosma & Mujica (2002) and Block et al. (2005) for earlier reviews or reviews covering sub-topics.

Bars are very common features. Eskridge et al. (2000), using a statistically well-defined sample of 186 disc galaxies from the Ohio State University Bright Spiral Galaxy Survey, find that 56% are strongly barred in the H band, while another 16% are weakly barred. Grosbøl, Patsis & Pompei (2002), using a smaller sample of 53 spirals observed in the K band, find that about 75% of them have bars or ovals.

In this paper I will discuss a number of results I have obtained recently on the formation and the dynamical evolution of bars. In particular, I will discuss the effect of angular momentum exchange within the galaxy, the role of the halo, the orbital structure in barred galaxies and the effect of a central mass concentration on the evolution.

## 2 Orbital structure in barred galaxies

The first step towards understanding the dynamics of a given structure is to understand its main families of periodic orbits. Indeed, if a periodic orbit is stable, it can trap around it regular orbits of similar orientation and morphology. On the other hand, unstable periodic orbits introduce chaos. A growing body of evidence shows that chaotic orbits can indeed be a considerable fraction of the total and that they contribute significantly to the morphology and to the kinematics of bars (e.g. Binney 1982; Athanassoula et al. 1983; Pfenniger 1984b; Teuben & Sanders 1985; Hasan & Norman 1990; Patsis, Athanassoula & Quillen 1997; Contopoulos 2002; El-Zant & Shlosman 2002, 2003).

### 2.1 Periodic orbits

The basic families of periodic orbits were calculated first in 2D models. Due to restricted computing power, the earlier studies were rather limited (e.g. de Vaucouleurs & Freeman 1972, Michalodimitrakis 1975). The first extensive study was done by Contopoulos & Papayannopoulos (1980), who used a very simplified potential to calculate orbits both inside and outside corotation (hereafter CR). They called the main family  $x_1$  and showed that within CR it is elongated along the bar. They also presented the banana-like Lagrangian orbits, around the Lagrangian points  $L_4$  and  $L_5$ , the family  $x_2$  of central orbits elongated perpendicular to the bar and the retrograde family  $x_4$ . Athanassoula et al. (1983) extended this work using a much more realistic bar potential, namely the Ferrers' potential (Ferrers 1877). Unfortunately their nomenclature is different from that of Contopoulos & Papayannopoulos (1980), the main family being called here  $B$ , the perpendicular one  $A$  and the retrograde one  $R$ . They confirmed that the  $B$  ( $x_1$ ) family is the backbone of the bar. They used surfaces of section to show that most regular quasi-periodic orbits are trapped

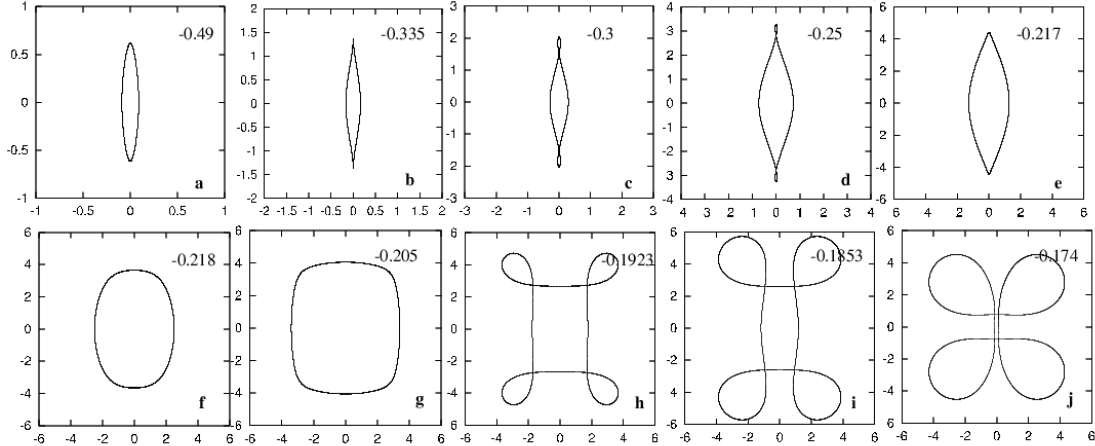


Figure 1: Examples of  $x_1$  orbits. The bar is oriented along the  $y$  axis and has a semi-major axis equal to 6 length units. The Jacobi constant, given in the upper right corner of each panel, increases from left to right and from top to bottom. From Skokos, Patsis & Athanassoula 2002, Monthly Notices of the Royal Astronomical Society, 333, 847, Blackwell Publ.

around family  $B$  ( $x_1$ ) or around the main retrograde family  $R$  ( $x_4$ ). They also showed that more massive and/or more eccentric bars introduce more chaos.

Figure 1 (from Skokos, Patsis & Athanassoula 2002a) shows a sequence of orbits of the  $x_1$  family. Following them in order of increasing Jacobi constant, we see a morphological sequence, first discussed by Athanassoula (1992). Namely the orbits first become cuspy at the apocenter, where, for yet larger energies, they acquire two loops, one at each apocenter. At yet higher energies these two loops disappear and the orbits become oval-like and then rectangular-like. At the largest energies the orbits form four loops, one at each of the four corners of the rectangular-like shape.

More than half of the orbits displayed in figure 1 close after one revolution around the center and two radial oscillations. They are thus resonant 1:2 orbits and are often referred to as such. At higher energies, however, the orbits close after one rotation and 4 (or more) radial oscillations. Such orbits are often considered as members of the  $x_1$  family, but can also be called 1:4, 1:6, or in general 1: $n$ , orbits.

3D studies showed that the orbital structure is much richer and more complicated. Pfenniger (1984a) initiated such studies and showed that there are several families of 3D orbits, bifurcated at the vertical resonances of the main planar family. This work was supplemented and extended in a series of four papers (Skokos, Patsis & Athanassoula 2002a, b; Patsis, Skokos & Athanassoula 2002, 2003). I will briefly recall here some results from these papers that are relevant to the subjects discussed here. I will also follow their notation.

The backbone of 3D bars is the  $x_1$  tree, i.e. the  $x_1$  family plus a tree of 2D and 3D families bifurcating from it (Skokos, Patsis & Athanassoula 2002a, b). These 3D families

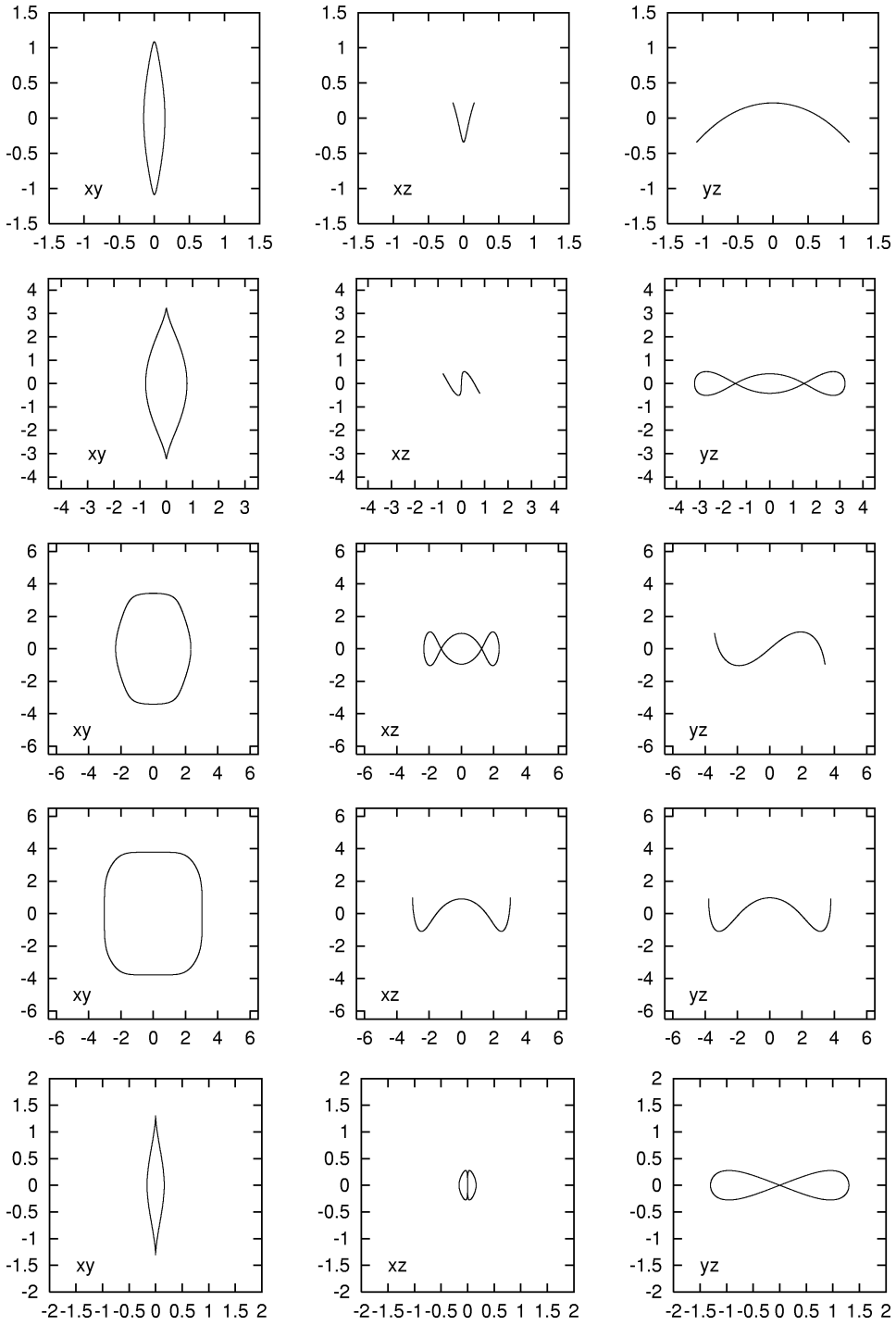


Figure 2: Three orthogonal views of characteristic 3D orbits in barred galaxies. The bar is oriented along the  $y$  axis and has a semi-major axis equal to 6 length units. From top to bottom, these orbits are members of the families x1v1, x1v3, x1v4, x1v5 and x1v2.

are called  $x1vn$ , where  $n$  is the order with which they are bifurcated in the fiducial model. Thus the family which bifurcates at the lowest energy is  $x1v1$ , followed by  $x1v2$ , then  $x1v3$  etc. Characteristic orbits from these families in the fiducial model of Skokos, Patsis & Athanassoula (2002a) are given in figure 2. The first four (from families  $x1v1$ ,  $x1v3$ ,  $x1v4$  and  $x1v5$ ) are stable. The last one (from family  $x1v2$ ) is unstable. A comparison of figures 1 and 2 clearly shows the morphological similarity of the orbits of the  $x_1$  family in the 2D problem and the  $(x,y)$  projection of the  $x1vn$  orbits. On the other hand, the  $x1vn$  orbits extend well out of the equatorial plane. It is thus the trapping around the periodic orbits of the  $x_1$  tree that will define the shape of the bar in the equatorial plane, as well as its thickness perpendicular to it.

Skokos, Patsis & Athanassoula (2002a) found also 3D families of banana-like orbits around the  $L_4$  and  $L_5$  Lagrangian points. Considerable sections of the families are stable. More surprising, they also found *stable* periodic orbits around the unstable Lagrangian points  $L_1$  and  $L_2$ . The family is planar, starts unstable, but turns stable at larger energy values.

## 2.2 Chaos and how to measure it

Galaxies are systems that contain both order and chaos, i.e. they have both ordered and chaotic orbits. For 2D systems for which there is a rotating frame of reference in which the energy is an integral of the motion, the most straightforward way of distinguishing between the two is to use surfaces of section. Even idealised galaxies, however, often do not fulfill these conditions. Thus many methods for measuring chaos have been so far proposed (see Contopoulos 2002 for a review).

I will here use a method proposed by the person we are honouring in this meeting, Henry Kandrup, and his collaborators (Kandrup, Eckstein & Bradley 1997). By Fourier transforming a quantity related to the orbital coordinates, e.g. the cylindrical radius  $R$ , or the complex quantity  $x + iy$ , one obtains a spectrum. If the orbit is regular, all the power of the spectrum lies in few, well defined peaks, while, if the orbit is chaotic, there is a continuum of frequencies within which the power is distributed. This is illustrated in figure 3, which shows two orbits, one regular and the other chaotic, and their corresponding spectra.

Kandrup et al. (1997) define as the complexity  $n(k)$  of an orbit, or, more precisely, of an orbital segment, the number of frequencies in its discrete Fourier spectrum that contain a fraction  $k$  of its total power. Regular orbits will have small values of  $n(k)$ , as opposed to chaotic orbits which will have big values. The optimum value for  $k$  depends on the size of the orbital segment and the frequency of the sampling. For the cases I discuss in this paper, I use potentials from  $N$ -body simulations and consider 65536 time steps in 40 bar rotations. For such cases, Misiriotis & Athanassoula (in preparation) found  $k = 0.98$  to

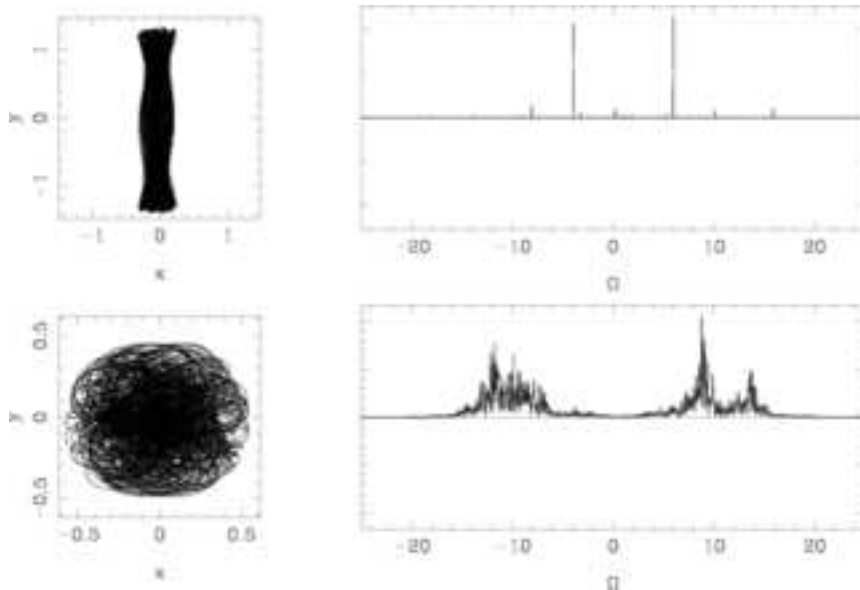


Figure 3: The  $(x,y)$  projection of two orbits (left panels) and the amplitude of the corresponding power spectra of  $x + iy$  (right panels). The orbit described in the upper panels is regular, while the one in the lower panels is chaotic.

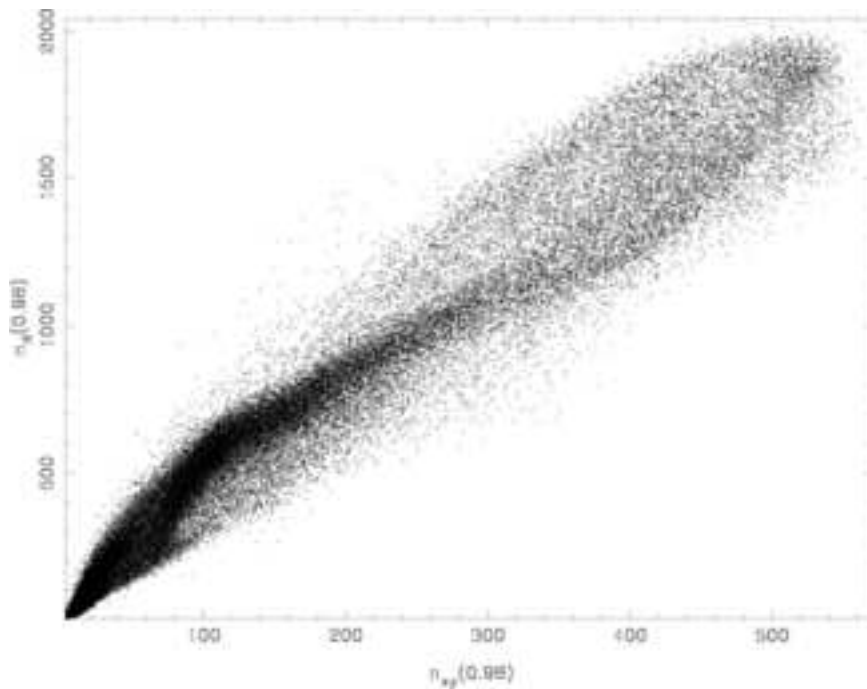


Figure 4: Complexity of disc orbits obtained from the  $R$  spectrum as a function of that obtained, for the same orbits, from the  $x + iy$  spectrum.

be the optimum value. Other large values would have also been reasonable choices, since the Rank-Order correlation coefficient of the complexities obtained using  $k$  values between 0.90 and 0.99 is always larger than 0.9 (Misiriotis & Athanassoula, in preparation). This confirms the result found by Kandrup et al. (1997) for a different potential and under different conditions. Misiriotis & Athanassoula (in preparation) also found a strong correlation between the complexity found from the  $x + iy$  spectrum and that calculated from the  $R$  spectrum. This is illustrated in figure 4, for the disc orbits of a simulation with a strong bar. The Rank-Order correlation coefficient of these two quantities is, in this case, 0.99. Kandrup et al. (1997) found strong correlations of the complexity with the short term Lyapunov exponents, often used to measure chaos. They thus concluded that the complexity  $n(k)$  is a robust quantitative diagnostic of chaos. It is particularly straightforward to apply to  $N$ -body simulations and it executes very fast, so that it can be applied to a very large number of orbits and simulations. I will thus adopt it for the estimates presented here. This definition shares the shortcoming of other chaos definitions. i.e. there is no clear dividing line between chaotic orbits and regular, but very complex ones.

### 3 The effect of the halo

$N$ -body simulations of the early seventies (Miller, Prendergast & Quirk 1970; Hohl 1971) already showed that bars form spontaneously in galactic discs. At that time the observational evidence for the existence of dark haloes around individual galaxies was hardly compelling, so the discs in these simulations are self-gravitating. Only a few years later haloes were propelled into the center of scientific discussions. Ostriker & Peebles (1973) were the first to check the effect of a heavy halo on the bar instability and found it to be stabilising. Although the number of particles in their simulations did not exceed 500, their work is very insightful. They introduced the parameter  $t_{op}$ , which is the ratio of kinetic energy of rotation to total gravitational energy and they concluded that halo-to-disc mass ratios of 1 to 2.5 and an initial value of  $t_{op} = 0.14 \pm 0.03$  are required for stability. Several later papers (e.g. Efstathiou, Lake & Negroponte 1982; Athanassoula & Sellwood 1986; Bottema 2003) confirmed the stabilising tendency of the halo. Yet, as we will see in the next section, this is an artifact, due to the fact that these simulations were either 2D, or had a rigid halo, or had too few particles. Thus the halo was not properly described and stabilised the bar. The first doubts about an entirely passive role of the halo component were voiced by Toomre (1977).

The importance of a live halo in order to model correctly the evolution of a barred galaxy was clearly demonstrated by Athanassoula (2002, hereafter A02). Two simulations are compared in this paper. They have initially identical disc components and their haloes have initially identical mass distributions. However, in one of the two simulations the halo

is live, i.e. it is composed of particles, while in the other it is rigid, i.e. it is an imposed potential. Thus in the former simulation the halo can absorb angular momentum, while in the latter it can not. The difference in the evolution is very striking. The simulation with the live halo grows a very strong bar, which, when seen side-on, has a strong peanut shape. On the contrary, the simulation with the rigid halo has a very mild oval in the innermost regions, and hardly evolves when seen edge-on. The large difference between the results of the two simulations argues strongly that the angular momentum absorbed by the halo can be a decisive factor in the evolution of the bar component.

Athanassoula & Misiriotis (2002, hereafter AM02) studied the morphology, photometry and kinematics of the bar as a function of the central concentration of the halo. They found that the bars that grow in centrally concentrated haloes are stronger, longer and thinner than bars in less centrally concentrated haloes, as can also be seen in figures 5 and 6. AM02 called the former MH-types and the latter MD-types. MH-type bars grow initially slower than MD-types, in good agreement with what was found by previous studies (e.g. Athanassoula & Sellwood 1986). They reach, however, higher amplitudes. Their face-on isodensity contours are rectangular-like, while the corresponding ones in MD-types are more elliptical-like. Their  $m = 4, 6$  and even 8 Fourier components of the density are well out of the noise and their amplitude reaches a considerable fraction of the corresponding  $m = 2$ , contrary to MD-types in which the  $m = 6$  and 8 are negligible. The density profile along the bar major axis (face-on view) also differs in the two types of bars. In MH-types it is rather flat, with an abrupt drop at the end of the bar, while in MD-types it drops near-exponentially with distance from the center (figure 5 in AM02). Bars in MH-type models often have ansae and/or an inner ring, which is elongated, but not far from circular and has the same major axis as the bar, as inner rings observed in barred galaxies (Buta 1986). Their side-on<sup>a</sup> shape evolves first to boxy and then to peanut or X shape, in contrast to the MD-types for which the side-on outline stays boxy. The side-on velocity field of MH-types shows cylindrical rotation, while the MD-types do not. More information on these properties can be found in AM02.

It is worth noting (see also Athanassoula 2003b) that a number of the properties of the MH-type galaxies are found in early type bars. Thus, early type bars are longer than late type ones (Elmegreen & Elmegreen 1985). They often have ansae (Sandage 1961) and flat projected light profiles along the bar major axis, in contrast to late type bars which have more sharply falling profiles (Elmegreen & Elmegreen 1985; Ohta, Hamabe & Wakamatsu 1990; Ohta 1996). Strong early-type bars have rectangular-like outlines (Athanassoula et al. 1990) and  $m = 6$  and 8 Fourier components of the density of considerable amplitude, contrary to late type bars, where these components are negligible (Ohta 1996).

From the results summarised in this section, it becomes clear that, contrary to previous

---

<sup>a</sup>The side-on view is the the edge-on view in which the line of sight is along the bar minor axis. The end-on view is the edge-on view in which the line of sight is along the bar major axis.

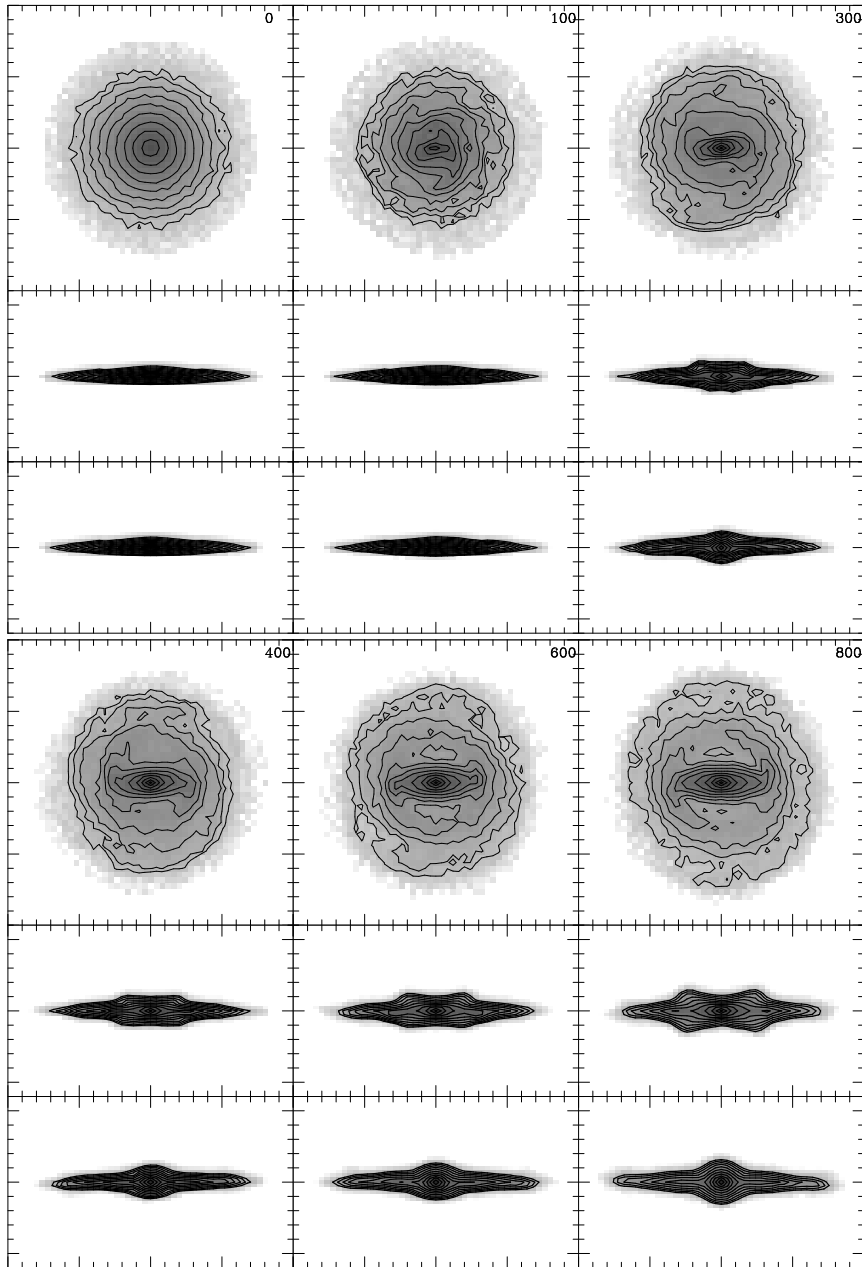


Figure 5: Formation of a bar in an initially axisymmetric disc. The model is of MH-type. The upper and fourth rows give the face-on views; the second and fifth ones the side-on views and the third and sixth rows the end-on views. Time increases from left to right and from top to bottom and is given in the upper right corner of each face-on panel. Here and elsewhere in this paper, times are given in computer units as defined by Athanassoula & Misiriotis (2002).

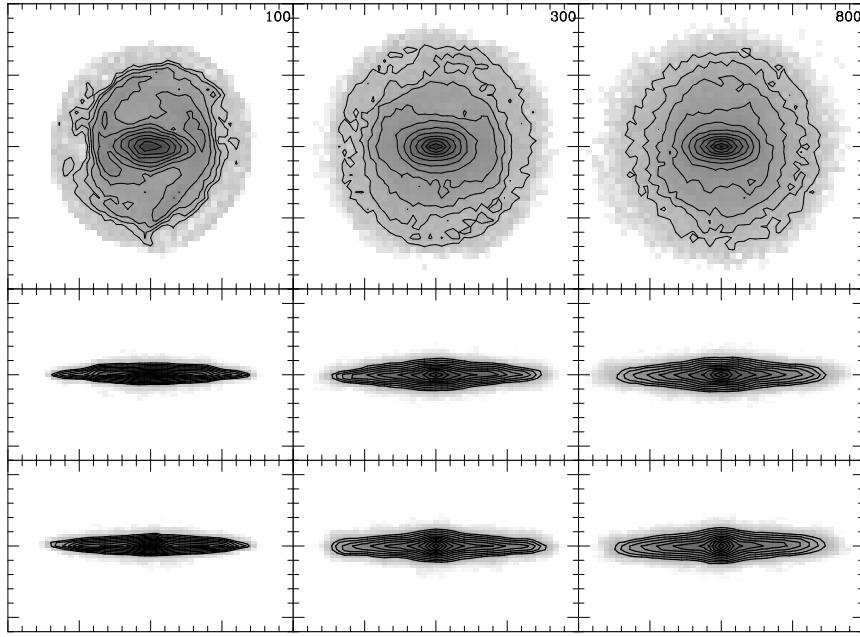


Figure 6: Formation of a bar in a disc dominated model (MD-type). The layout is as in Fig. 5.

beliefs, a *live* halo can *help the bar grow*, so that bars growing in galaxies with responsive massive haloes can become stronger than bars growing in disc-dominated galaxies. This marks the end of a paradigm.

## 4 Angular momentum exchange

The secular growth of the bar component in isolated galaxies is driven by the angular momentum redistribution within them. This was initially proposed, for galaxies with no spheroidal component, by Lynden-Bell & Kalnajs (1972), and later extended to galaxies with haloes and/or bulges by Athanassoula (2003, hereafter A03). Angular momentum is emitted mainly by near-resonant stars in the inner disc (namely at inner Lindblad resonance, hereafter ILR), or at higher order inner resonances (1: $n$ ) and, if the perturbation is growing, also by non-resonant stars in that region. It is absorbed mainly by stars at near-resonance in the outer disc – CR and outer Lindblad resonance (hereafter OLR) – and at all resonances of the halo. The latter effect of the halo can be followed analytically if the distribution function of this component depends on the energy only. A full analytical treatment of other distribution functions is not yet available, but a preliminary analysis of models with non-isotropic velocity distribution (Fuchs & Athanassoula, in preparation) indicates that these could drive an even stronger bar growth.

The net result is a transport of the angular momentum outwards. Colder material can emit/absorb more angular momentum than hotter material. Thus the halo is less responsive

than the disc per equal amount of resonant mass. There is, however, not much material in the outer disc, where the density is very low, while the halo can be very massive. It can thus be that the halo absorbs more angular momentum than the outer disc, and this has proven to be the case in many  $N$ -body simulations, as will be discussed in the next section. Since the bar is a negative angular momentum ‘perturbation’ (Kalnajs 1971; Lynden-Bell & Kalnajs 1972), by losing angular momentum it becomes stronger.

The Lynden-Bell & Kalnajs (1972) formalism and its extension to include spheroidal components (A03) were able to predict successfully which resonances emit and which absorb angular momentum. Extending it, however, beyond such qualitative results to obtain a quantitative estimate of the bar growth, is not possible, since, as stressed by Weinberg (2004), it assumes that the perturbations grow slowly over a very long time and that transients can be ignored. For this reason, quantitative estimates of the bar growth have, so far, only been obtained numerically.

Tremaine & Weinberg (1984) also studied the effect of the resonances, focusing on the effect of the angular momentum exchange on the bar pattern speed. They showed that the dynamical friction on the bar arises from stars which are near-resonant with the rotating bar. They derived an analogue of Chandrasekhar’s formula (Chandrasekhar 1943) for spherical systems, valid when the angular velocity of the bar does not change too slowly. Weinberg (1985) calculated that the angular momentum exchange between the bar and the halo will cause a considerable slow-down of the former within a few bar rotations. As we will see in the next section, bars in  $N$ -body simulations also present such a slow-down (Little & Carlberg 1991a, 1991b; Hernquist & Weinberg 1992; Athanassoula 1996; Debattista & Sellwood 2000; A03; O’Neill & Dubinski 2003; Valenzuela & Klypin 2003), in good qualitative agreement with the analytical results. A quantitative comparison may not be meaningful, because of the limitations underlying the theory, in particular the fact that theory has not treated so far both the change of pattern speed and the bar growth simultaneously.

## 5 Results from $N$ -body simulations

Contrary to real galaxies,  $N$ -body simulations are well suited for studying the angular momentum exchange within a galaxy. This has been one of the main goals of A02 and A03 and I will retrace here a number of the steps made in those papers.

A02 and A03 first checked that there is a considerable amount of near-resonant material in the halo component. This can also be seen, for a strong bar simulation, in the upper panels of figure 7, where I plot the mass per unit frequency ratio,  $M_R$ , as a function of the frequency ratio  $(\Omega - \Omega_p)/\kappa$ . Here  $\Omega$  is the angular frequency of the orbit,  $\kappa$  is its radial frequency and  $\Omega_p$  is the bar pattern speed. It is clear that the distribution is not uniform, and

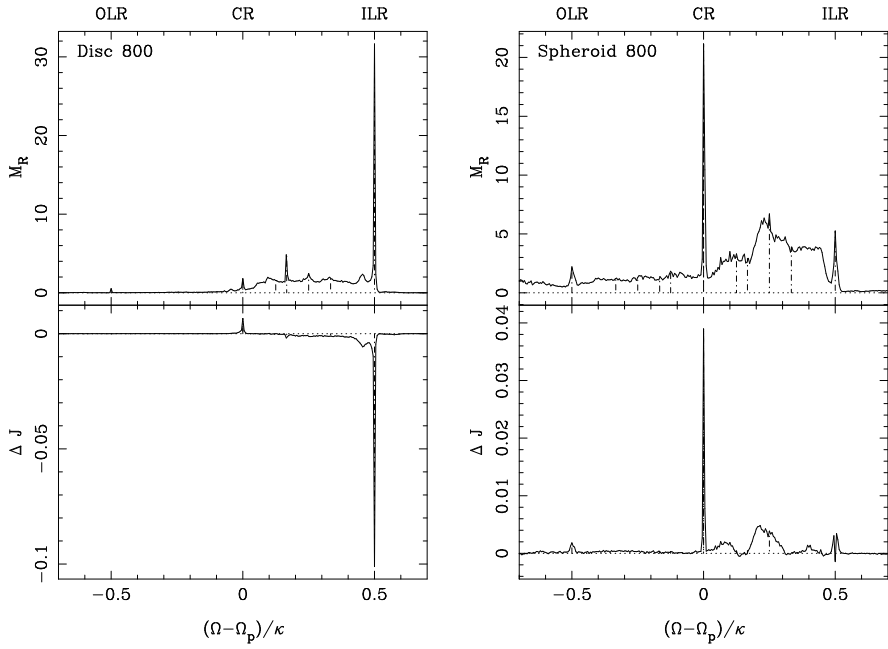


Figure 7: Resonances in the disc and the spheroidal component. The upper panels give, for the time  $t = 800$ , the mass per unit frequency ratio,  $M_R$ , as a function of that ratio. The frequency ratio is defined as  $(\Omega - \Omega_p)/\kappa$ , the ratio of the angular frequency in the frame in which the bar is at rest to the epicyclic frequency. The lower panels give  $\Delta J$ , the angular momentum gained or lost by particles of a given frequency ratio between times 500 and 800, as a function of that frequency ratio, calculated at  $t = 800$ . The left panels correspond to the disc component and the right ones to the spheroid. The vertical dot-dashed lines give the positions of the main resonances.

that its peaks are located at the main resonances. In all simulations, the disc has a strong peak at ILR, which is made of particles trapped around this resonance and constituting the backbone of the bar. Secondary peaks can be found at other resonances – as e.g. inner 1:3, inner 1:4, CR or OLR – whose existence and height varies from one simulation to another. More important, the halo component also shows similar peaks. The highest is at CR, while secondary peaks can be seen at ILR and OLR. Such peaks can be seen in all simulations I analysed, again with varying heights.

The bottom panels of figure 7 show the way the angular momentum is exchanged. For the disc component it is emitted from the region within the bar, and particularly the ILR, and absorbed at CR (and in some simulations also at OLR). However, the amount of angular momentum emitted is much more than what the outer disc absorbs. This is understood with the help of the bottom right panel, which shows that all the halo resonances absorb a considerable amount of angular momentum, much more so than the outer disc. A more complete discussion and analysis can be found in A02 and A03. Thus simulations confirm the angular momentum exchange mechanism suggested by the analytical work and show that the halo can be an important agent in this respect.

This also explains why strong bars can not grow in simulations with rigid haloes. Indeed, as initially discussed in A02, in such cases the halo can not take angular momentum from the bar and thus it limits bar growth. The difference between the bar strength in live and in rigid haloes should be larger in cases when the role of the halo in the angular momentum exchange is more important.

The global redistribution of angular momentum was followed in Debattista & Sellwood (2000), A03, O'Neill & Dubinski (2003) and Valenzuela & Klypin (2003) and shows clearly that angular momentum is taken from the disc by the halo. This is in good agreement both with the theoretical predictions and with the above more detailed analysis.

Simulations also show that the bar grows as a result of the angular momentum exchange, as expected from theory. As already discussed in the previous section, they show that the bar grows particularly strong if the halo can take from it considerable amounts of angular momentum. For such simulations, A03 found a clear correlation between the amplitude of the bar and the angular momentum taken by the halo.

Simulations also show that the bar slows down as a result of the angular momentum exchange, as expected from theory (Little & Carlberg 1991a, 1991b; Hernquist & Weinberg 1992; Athanassoula 1996; Debattista & Sellwood 2000; A03; O'Neill & Dubinski 2003; Valenzuela & Klypin 2003). Thus one would expect an anti-correlation between the strength and the pattern speed of the bar, and this was indeed established by A03, for a large number of simulations.

Theoretical arguments predict that the angular momentum emitted or absorbed at a given resonance depends not only on the density of matter there, but also on how cold the near-resonant material is. This is borne out by the simulations (A03). Indeed, if the disc is hot (i.e. has a high initial  $Q$ ) and/or the halo is very hot, then the bar does not grow to be very strong and does not slow down much, even in cases where the halo is very dense. Examples of this are given by A03.

The angular momentum exchange also determines the morphology of the bar (Athanassoula 2005). Simulations where only little angular momentum has been exchanged harbour either an oval or a very short bar. Ovals are mainly found in simulations with hot discs, while short bars are predominantly found in simulations with hot haloes. At the other extreme, in simulations in which a large amount of angular momentum is redistributed the bar is strong, resembling the MH model of AM02 (see also figure 5). As already discussed in section 3, such bars resemble the strong bars in early type barred galaxies. Thus one can argue that a considerable amount of angular momentum has been redistributed in such galaxies between the disc and the spheroidal component. This would be partly taken by the strong bulge component these galaxies have, and partly by their halo. Extreme cases of such galaxies are some examples of bar dominated early type discs presented by Gadotti & de Souza (2003), in which the disc is not a major component any more, since a very considerable fraction of its mass is now within the bar component.

I have so far taken into account only the disc and halo (and sometimes bulge) components. Yet the complete picture of angular momentum exchange can be more complicated. Galaxies (particularly late types) have also a gaseous disc component. This may give angular momentum to the bar, and thus decrease its strength (Berentzen et al. 2004). Furthermore, galaxies are not isolated universes, and thus can interact with their companions, or satellites. If the latter absorb angular momentum, then the bar can grow stronger than in the isolated disc (Berentzen et al. 2004). This is in good agreement with observational results that show that more bars can be found in interacting than in isolated galaxies (Elmegreen, Elmegreen & Bellin 1990).

In isolated galaxies, angular momentum can only be redistributed between the various components, i.e. there should be as much angular momentum absorbed as emitted. Thus a very massive and responsive halo that can absorb large amounts of angular momentum is not sufficient to ensure important angular momentum redistribution. This can indeed be limited by the amount of angular momentum that the inner disc can emit, so that, if the disc has a very low surface density and/or is very hot, little angular momentum will be exchanged. In other words, it is not useful to increase the capacity of the absorbers if the emitters do not follow, and vice versa. Similar arguments can constrain the position of CR. If this is located in the inner parts of the disc it will privilege the absorbers to the detriment of the emitters. This occurs in simulations where the halo absorption is limited so that the contribution of the outer disc is essential. On the contrary, a CR located in the outermost parts of the disc favours emitters. This ensures a maximum exchange in cases where the halo is capable of absorbing a lot of angular momentum.

## 6 A bar in the halo component

The halo evolves dynamically together with the disc. In simulations in which a considerable amount of angular momentum has been exchanged and which have thus formed a strong bar, the halo does not stay axisymmetric. It also forms a bar, or more precisely an oval, which I will call, for brevity, the halo bar to distinguish it from the bar in the disc component, which I will refer to as the disc bar. An example is seen in figure 8, which compares the morphology of the disc bar (upper panels) to that of the halo bar (lower panels). A very clear case of such a structure is also seen in figure 2 of Holley-Bockelmann, Weinberg & Katz (2003).

Halo bars are triaxial, but nearer to prolate than to oblate, with their minor axis perpendicular to the disc equatorial plane. Their axial ratio in this plane (ratio of minor to major axis) is considerably larger than that of the corresponding disc bar. It increases with increasing radius, so that halo bars tend to become axisymmetric in the outer parts. Since the change in axial ratio is very gradual, it is not easy to define precisely the end of the halo

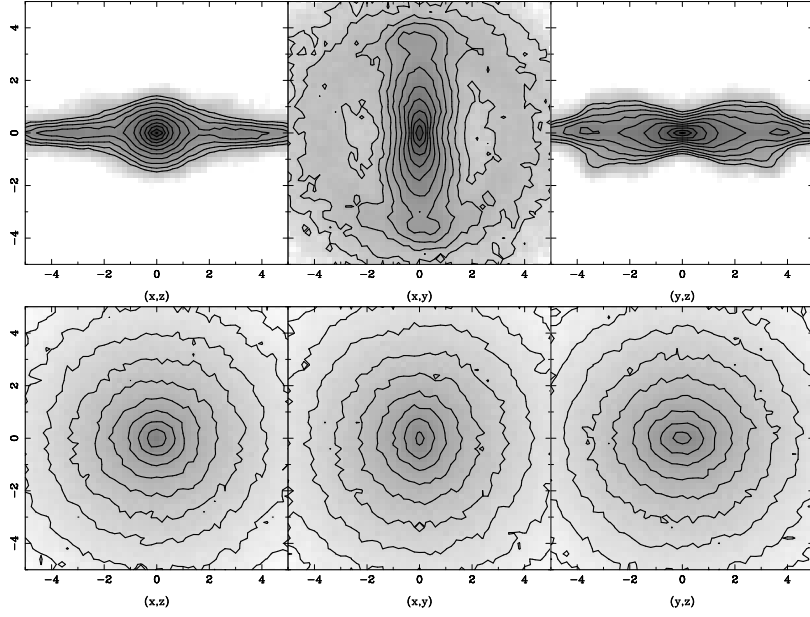


Figure 8: Three orthogonal views of the disc (upper panels) and halo components (lower panels). The central panel is a face-on view, while the two others are edge-on; side-on for the right panels and end-on for the left ones. Note that the halo component does not stay axisymmetric, but forms an oval in its inner parts, which I call the halo bar.

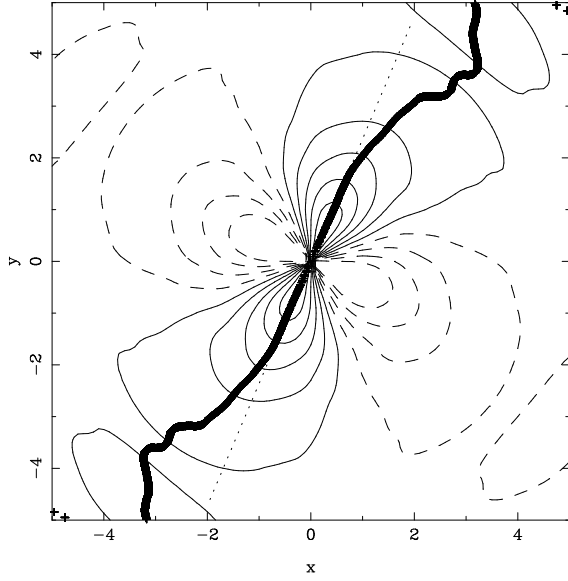


Figure 9: Isocontours of the  $l=2$   $m=2$  component of the halo mass distribution on the equatorial plane. Positive isocontours are given with solid lines and negative ones with dashed lines. The thick line shows the phase of the halo bar and the thin dotted line gives the position angle of the disc bar.

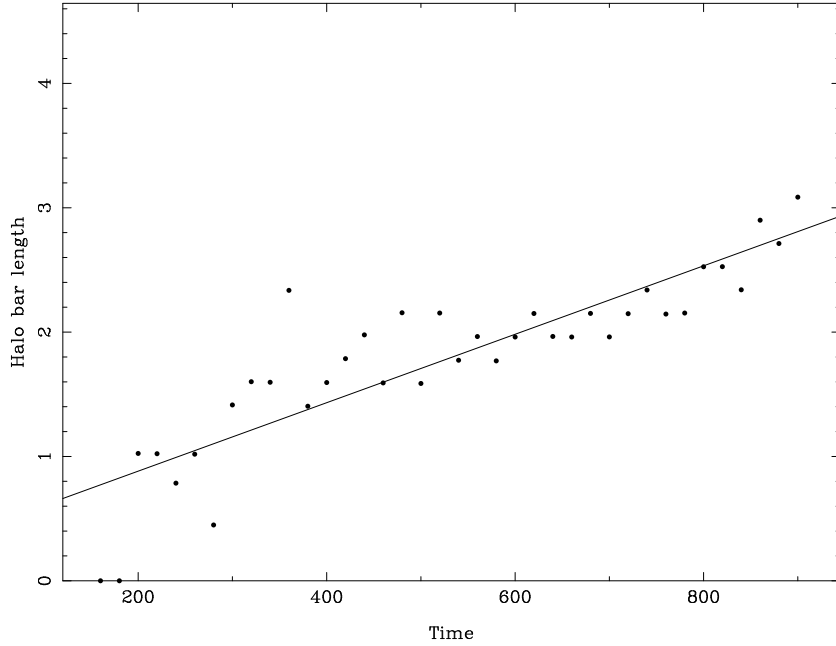


Figure 10: Length of the halo bar as a function of time. The solid line is a least square fit.

bar, and thus to calculate its length, so that any measurement will have a considerable error. It is clear, however, that it is always considerably shorter than the disc bar.

The phase and amplitude of the halo bar can be best studied with the help of a decomposition into spherical harmonics. The mass distribution of the  $l = 2$  and  $m = 2$  component on the equatorial plane, as obtained from such a decomposition (Athanassoula, in preparation), is given in figure 9. It shows clearly that in the inner parts, where the phase of the halo bar does not change much with radius, the halo bar has roughly the same orientation as the disc bar. This is true at all times after both bars have grown sufficiently to allow a relatively accurate measurement of their amplitude and phase. Closer examination, however, shows that the halo bar lags the disc bar slightly, by something like a couple of degrees in the innermost parts. This shift is always trailing and increases with increasing distance from the center. Thus the  $m=2$  component of the halo continues well outside the halo bar, trailing behind the disc bar, so that, after a certain distance, the structure can be described as a trailing very open spiral.

The length of the halo bar can be defined by setting a limiting value for the phase difference between the halo and the disc bar. It is given as a function of time for a simulation with a strong disc bar in figure 10. The spread in the measurements reflects the difficulty of defining precisely the end of the halo bar. Yet a least square fit shows clearly that the length of the halo bar increases with time. Comparison with similar data, but now for the disc bar, shows that the length of the halo bar increases slower than that of the disc bar.

I carried out such an analysis for a number of simulations in which the halo bar is

sufficiently strong so that its properties can be measured accurately. I find that the halo bar length correlates with the disc bar length and that the regression line changes with time, as would be expected since the disc bar grows faster than the halo bar. I found also correlations between the disc and the halo bar strengths, as well as between the ellipticity of the halo bar and its flattening towards the equatorial plane. More information on the halo bar properties and their relation with the disc bar properties will be given elsewhere (Athanassoula, in preparation).

## 7 Orbital structure in the disc and halo components

Studies of orbital structure in 3D barred potentials can give useful information on the families of periodic orbits, their stability and the morphology of their orbits. They can not, however, give information on how many orbits, if any, are trapped around a given periodic orbit family. This information is only available from  $N$ -body simulations. The orbital structure has been so far examined in simulations of 2D or 3D discs (Sparke & Sellwood 1987; Pfenniger & Friedli 1991; Berentzen et al. 1998), but never, so far, for their haloes. Yet, as discussed in sections 4 and 5, haloes also have near-resonant orbits, and thus should have an interesting orbital structure. I will here present some preliminary results on the orbital structure of the disc and halo components. I use a method which is, in several aspects, similar to that outlined in the above mentioned papers. Namely, at a given time well after the bar has grown, the potential and forces from a given simulation are calculated on a grid, which is sometimes further made bisymmetric, since most of the orbital families have that symmetry. The bar pattern speed at that same time is also calculated from the simulation. In the above mentioned papers, this information is used to calculate families of periodic orbits. Unfortunately, numerical noise, which is inherent in  $N$ -body simulations, limits such studies to few orbital families and makes stability analyses very difficult, if not impossible. Instead of this, I take the positions and velocities of 100 000 disc and 100 000 halo particles, drawn at random from the corresponding populations at the time at which the potential and pattern speed are calculated. I use these as initial conditions and follow the corresponding orbits for 40 bar rotations. Examining these orbits leads to a number of conclusions, some of which I will briefly discuss below. A more complete analysis, comparing several simulations, will be given elsewhere (Athanassoula, in preparation).

Of course, these orbits are not the same as those of the same particles throughout the simulation. The simulation orbits start off in an axially symmetric potential and evolve as the bar first forms and then evolves. During the formation phase the potential changes drastically with time, so that any results obtained in the way described above should be considered with great caution. The formation phase, however, is followed by a phase of calm secular evolution, in which the potential changes slowly with time. It is during this

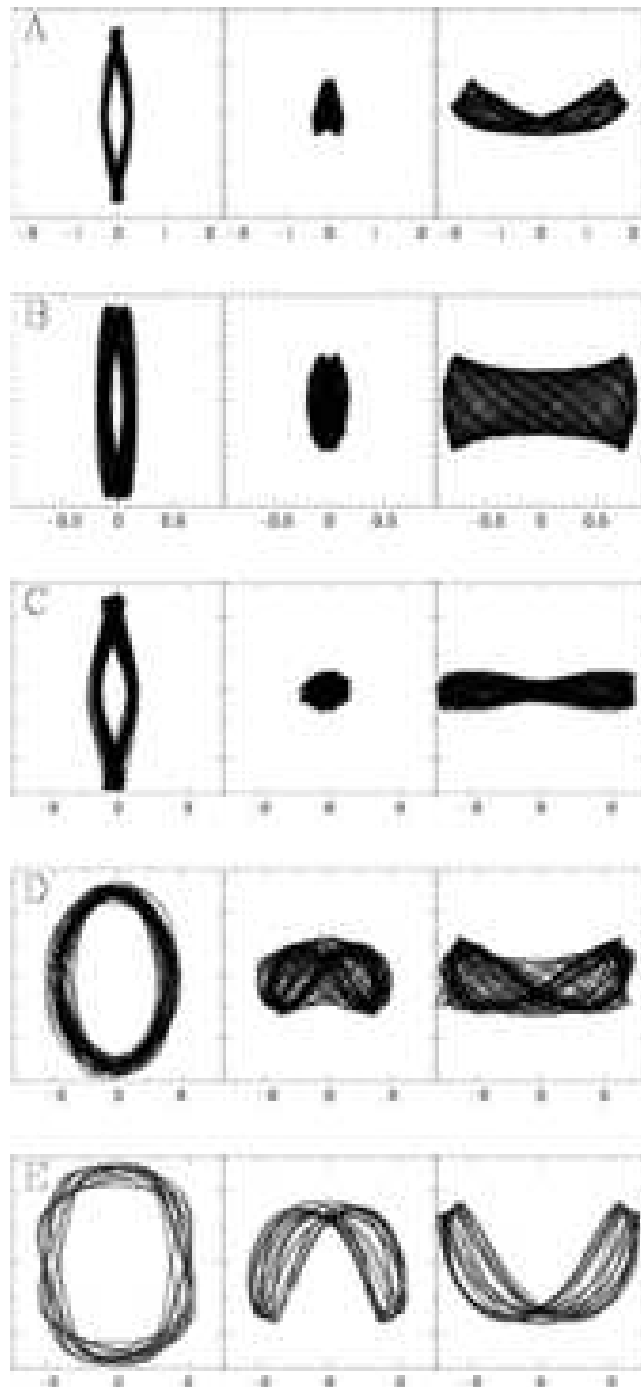


Figure 11: Six examples of typical halo near-ILR orbits. The  $(x, y)$ ,  $(x, z)$  and  $(y, z)$  projections are shown in the left, middle and right panels, respectively.

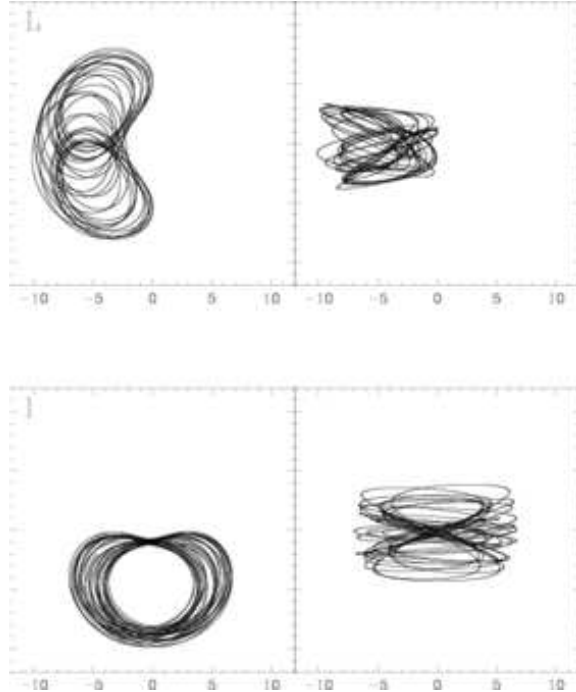


Figure 12: Two examples of typical halo near-CR orbits. The left panels give the face-on view,  $(x, y)$ , and the right ones the end-on view,  $(x, z)$ .

phase that the results obtained with the above method can be useful. The evolution of the potential brings about a change in the orbital structure. By studying this structure at a sequence of times, it is possible to get insight on its evolution. It should, of course, always be remembered that this is only an approximation, albeit the only one known so far that can give useful results. This approximation is also inherently present in any work on orbital structure, since such works have so far used only non-evolving potentials, whether these are taken from simulations, from observations, or from analytical models.

### 7.1 Morphology of halo near-resonant orbits

Typical halo orbits trapped around the periodic orbits of the  $x_1$  tree are shown in figure 11. They have been chosen as representative of types of orbits frequently encountered in the simulations presented here. The plots are made in a frame of reference in which the bar is at rest and the bar major axis is along the  $y$  axis.

Orbit A (upper panels) must be trapped around a stable periodic orbit having two oscillations in the  $z$  direction and two radial oscillations for each rotation, i.e. an orbit of the  $x1v1$  family, presumably resembling that shown in the upper panels of figure 2. Orbit B (second row) is presumably trapped around an orbit of the  $x1v1$  family *and* around its symmetric with respect to the disc equatorial plane. This orbit is located in the innermost

part of the halo.

Orbit C (third row) has a considerably smaller extent in the  $z$  direction. It is also more extended in the  $(x, y)$  plane, so that it has a considerably smaller aspect ratio seen side-on – i.e. in the  $(y, z)$  projection – than orbits A and B. Its shape is also different. Orbits A and B have a vertical extent which increases with increasing distance from the center, as is the case for the periodic orbits of the  $x1v1$  family. Thus the highest point in  $z$  is near the maximum  $y$  value, i.e. towards the tips of the  $(x, y)$  loop. On the contrary, the orbit in the third row seen side-on appears relatively flat for large  $y$  values, i.e. for large  $y$  values the  $z$ -extent does not increase with distance from the center, but stays roughly constant.

Orbit C can have two possible origins. The first possibility is that it is trapped around an  $x1v2$  periodic orbit (see e.g. the last row of panels of figure 2). This family has members with a similar orbital shape and extent to orbit C. It was, however, found to be unstable in the models studied so far (Skokos et al. 2000a, b) and thus cannot trap orbits around it. Changing the values of the parameters of the Skokos et al. models, it is possible to find cases which have an  $x1v2$  family with a stable section, but this is of a very short extent in all the cases examined (Patsis, private communication). Of course the potential in the simulations may not be well described by one of the models discussed by Skokos and collaborators and thus could have considerable differences in its orbital stability properties.

The second alternative is that orbits such as C are trapped around periodic orbits of the  $x1v4$  family. An example is given in the third row of panels of figure 2. An orbit trapped around two periodic orbits of this family, which are symmetric with respect to the equatorial plane, will look like orbit C and have the right shape and extent. It will be possible to distinguish between the two alternatives only after a complete study of the orbital structure has been made.

Orbits such as D, although rather frequent, are even more difficult to classify. Seen face-on, such orbits show a simple oval, with no cusps or loops at its tips. The edge-on views, however, reveal that the maximum  $z$  displacement is not at the tips of the oval, but considerably displaced. Again there are two possible alternatives as to the origin of such orbits.

The first alternative is that this is due to a local twist of the isodensities, which affects the edge-on, but not the face-on view. Such a displacement is seen e.g. in the  $x1v4$  periodic orbits (third row of panels of figure 2), even in cases where the isodensities have no twist.

The second alternative is that orbit D is trapped around a member of a higher multiplicity family bifurcating from the  $x_1$ , most probably one of multiplicity two. Such periodic orbits close after two rotations and four radial oscillations and thus can not be distinguished from those of the  $x_1$  by their frequency ratio. They had been found also in the models of Skokos et al., but were not discussed at length since those papers concentrated on periodic orbits of multiplicity 1. Orbit E, in the lowest row of panels of figure 11, argues yet stronger about its link with a periodic orbit of multiplicity 2. Such orbits are rather frequent amongst

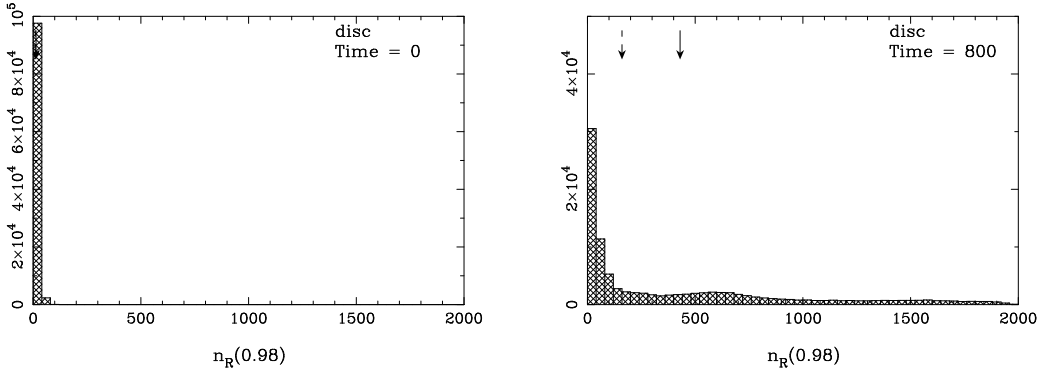


Figure 13: Number of disc orbits as a function of the complexity index  $n_R(0.98)$ . The left panel corresponds to the initial time and shows that all orbits are regular, i.e. have small complexity. The right panel corresponds to a time after a strong bar has grown and shows that many orbits have acquired very high complexity, i.e. have become chaotic. The solid-line and dashed-line-arrows give the mean and the median values, respectively.

the ones having a 1:2 frequency ratio and this argues that families with multiplicity higher than 1 should be considered in future orbital studies,

The orbits in figure 12 are ‘banana-like’. The one in the first row orbits around the  $L_4$ , or  $L_5$ , Lagrangian point and must be trapped around a long period banana orbit (Contopoulos & Grosbøl 1989). The example in the second row orbits around the  $L_1$ , or  $L_2$ , Lagrangian point. Although these points are known to be unstable (e.g. Binney & Tremaine 1987), Skokos et al. found a family whose members orbit around  $L_1$ , or  $L_2$ , and has considerable stable parts, They called it  $l_1$ . The morphology of the orbits of this family resembles that of the short period orbits around  $L_4$ , or  $L_5$ , rotated by  $\pi/2$ . The shape and orientation of orbit  $l$  (second row of figure 12) shows that it must be trapped around a periodic orbit of the  $l_1$  family.

In general, the shapes of the orbits of the halo near-resonant particles are similar to the corresponding disc ones. Although this might seem strange at first glance, it should in fact have been expected, since the periodic orbits are characteristic of the total potential, i.e. they are the same for the disc and the halo.

## 7.2 Fraction of chaotic orbits

The amount of chaos as a function of bar strength has already been addressed by Athanassoula et al. (1983), with the help of surfaces of sections. These authors plotted the fraction of the area of the surfaces of section which is covered by chaotic orbits as a function of the bar mass and axial ratio. They found that there is a clear trend, in the sense that stronger

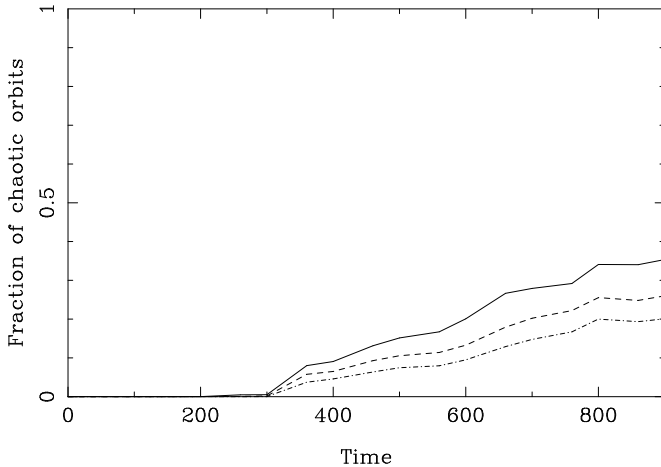


Figure 14: Fraction of the disc orbits that have a complexity above a given threshold as a function of time for a simulation with a strong bar. The three thresholds are 100 (solid line), 150 (dashed line) and 200 (dot-dashed line).

bars have a larger part of their surfaces of section covered by chaotic orbits. This was confirmed by Teuben & Sanders (1985), for a different model. Although very indicative, these results do not give a clear estimate of the amount of chaos in barred galaxies. Indeed, they do not take into account the time spent by an orbit between two consecutive crossings of the surface of section (e.g. Binney, Gerhard & Hut 1985) and, most important, they have no way of determining whether a given regular or chaotic orbit is populated, or not.

This information can only be obtained from  $N$ -body simulations. I have thus calculated the complexity of 100 000 disc particles, and 100 000 halo particles, taken at random from the corresponding population, and that for several times during the evolution. Initially, by construction, both the disc and the halo are axisymmetric, and there is no chaos in either component. This is, however, introduced gradually as the bar first forms and then becomes stronger with time, so that towards the end of the simulation there is a considerable fraction of chaotic orbits. This is seen, for the disc orbits, in figure 13. This shows, in form of a histogram, the number of disc particles as a function of their complexity, both initially and for a time towards the end of the simulations. We note that the distribution acquires a considerable tail towards complex/chaotic orbits.

The evolution of the number of disc chaotic orbits with time is further examined in figure 14. For this, I plot the number of orbits with complexity above a given threshold as a function of time. Before the bar forms there are no chaotic orbits, as expected. As the bar grows, the amount of chaos increases and, at the end of the simulation, nearly one third of

the disc orbits have a complexity higher than 100.

### 7.3 Where were the halo near-resonant particles initially?

Where do the halo particles at (near-) resonance originate from? Do all particles have equal probability of getting trapped at a resonance during the evolution, or are there preferred targets? To answer this question I first found the particles which are at (near-) resonance at a time well after the bar has formed and then traced them back to the initial conditions. I could thus compare the distribution of their main properties (cylindrical and spherical radius, distance from the equatorial plane,  $z$  component of the velocity and of the angular momentum, kinetic energy etc) with that of all the particles in the halo, both taken at  $t = 0$ . For CR, which is well populated and for which it is thus easy to make statistical tests, a Kolmogorov-Smirnov test shows beyond doubt that the two populations are not identical, i.e. that the particles which at later times are at CR are not initially randomly chosen from the initial halo population. The particles that will later get trapped at CR do not come initially from the innermost and outermost regions. Instead, they have preferentially intermediate cylindrical and spherical radii. They have preferentially (absolutely) smaller values of  $v_z$  and considerably larger values of  $J_z$ .

## 8 The effect of a central mass concentration on a bar

Central mass concentrations (hereafter CMCs) can be hazardous for the growth and even for the existence of a bar. This was first discussed by Hasan & Norman (1990) and Hasan, Pfenniger & Norman (1993), who studied the orbital structure in a rigid potential with both a bar and a CMC. They showed that the CMC alters the stability of the  $x_1$  orbits, making them largely unstable and thus came to the conclusion that a CMC can destroy the bar if it is sufficiently massive and/or sufficiently centrally concentrated. This work was extended with the help of  $N$ -body simulations first by Norman, Sellwood & Hasan (1996) and later by Hozumi & Hernquist (1998, 1999, 2004) and by Shen & Sellwood (2004). All three groups used  $N$  body simulations with live discs and rigid haloes. In all cases the CMC was introduced gradually, in order to avoid transients.

Seen the important role that the response of the halo can play on the evolution of barred galaxies, Athanassoula, Lambert & Dehnen (2005) revisited this problem, now using a live halo, and I will here summarise some of their results. They find that the effect of the CMC depends drastically on the model. This is illustrated in figure 15, which compares the effect of identical CMCs (of mass 0.05 and radius 0.01 for the middle panels, and for mass 0.1 and radius 0.01 for the lower panels) on two different barred galaxy models. The left column corresponds to an MH-type model, and the right one to an MD-type model. The difference

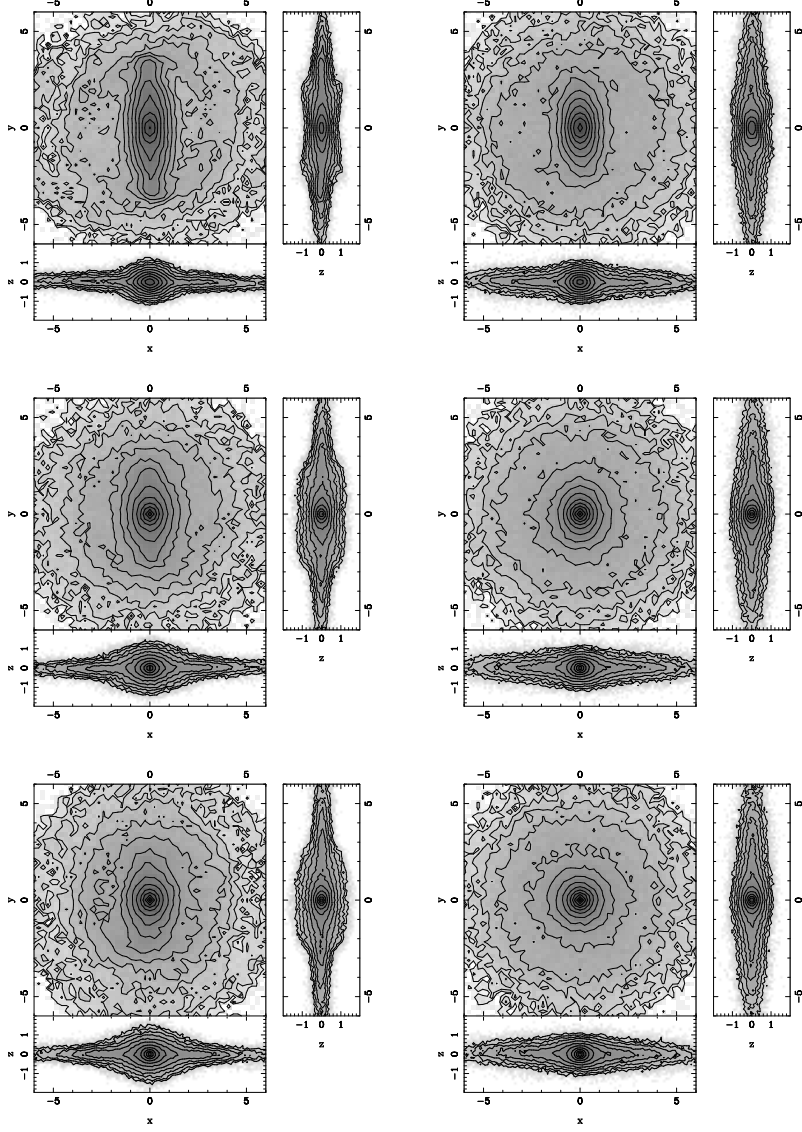


Figure 15: Effect of a CMC. The left panels correspond to MH-type models and the right ones to MD-type models. The upper panel shows the disc component at the time the CMC is introduced and the other two at  $\Delta T = 300$  later. The mass of the CMC is 0.05 for the middle panel and 0.1 for the lower one. Each sub-panel shows one of the three orthogonal views of the disc component. The right sub-panel gives the edge-on side-on view, the lower left one gives the edge-on end-on view and the upper left one gives the face-on view. The projected density of the disc is given by grey-scale and also by isocontours (spaced logarithmically).

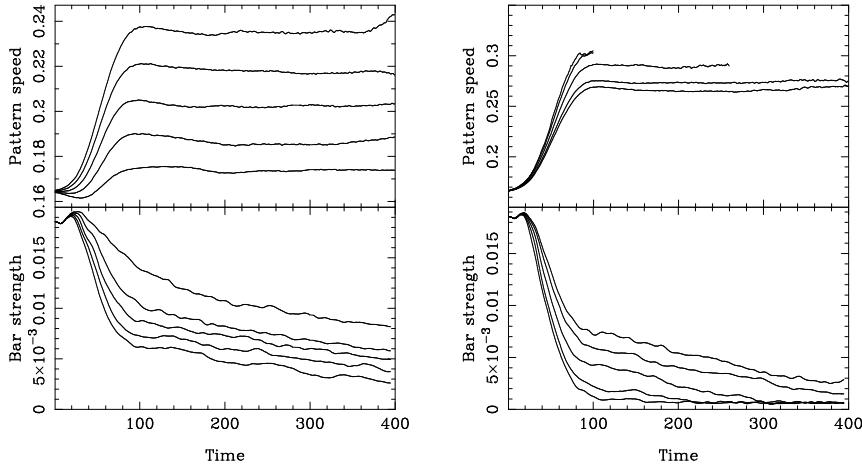


Figure 16: Pattern speed of the bar as a function of time (upper panels). For comparison, I plot in the lower panels a measure of the bar strength (the maximum value of the amplitude of the  $m = 2$  component of the mass distribution), also as a function of time. The left panels refer to a series of simulations with different CMC mass (from top to bottom in the lower panel and from bottom to top in the upper one : 0.01, 0.02, 0.03, 0.04, 0.05; all with a CMC radius of 0.01), while the right panels correspond to a series of simulations with different CMC radius (from top to bottom in the upper panel and from bottom to top in the lower one : 0.01, 0.02, 0.05, 0.08, 0.1; all with a CMC mass of 0.1). In all cases the CMC is introduced gradually in the first 100 time units.

is quite important. These CMCs decrease the strength of the bar in the MH-type models, but fully destroy it in MD-type ones. This figure also shows that the lowering of the bar strength is due to a decrease of the bar length and to more axisymmetric innermost parts. The latter can be understood since this is the vicinity of the CMC.

This difference between MH-type and MD-type models could be due to the role of the halo in the two cases. Indeed, in the MH-type haloes the inner resonances in the halo are more populated, so that the halo can absorb more angular momentum, compared to MD-type haloes (A03). This extra angular momentum is taken from the bar and will, as discussed in sections 4 and 5, tend to increase its strength and will work against the CMC, whose effect will thus be lessened. This is indeed what the simulations of Athanassoula et al. (2005) show.

The CMC also affects the vertical structure of the bar. Figure 15 shows that in MH-type models the peanut initially seen in the side-on view is converted to a boxy or elliptical-like shape. The radial extent, however, of this vertically protuberant part stays roughly the same. The CMC in the MD-type bar destroys the boxiness of the side-on view.

The CMC also causes an increase of the bar pattern speed. This is not always easy to measure, since, due to the CMC, the bar amplitude is severely decreased. It is, nevertheless, clear for the two sequences of simulations, compared in figure 16. This effect is in agreement with the anti-correlation between the bar strength and pattern speed, found in

**Acknowledgments** It is a pleasure to thank many friends and colleagues for interesting and motivating discussions, in particular A. Bosma, M. Bureau, G. Contopoulos, W. Dehnen, A. Misiriotis, P. Patsis, M. Tagger, N. Voglis, G. Aronica, I. Berentzen, K. Freeman, B. Fuchs, K. Holley-Bockelmann, A. Kalnajs, A. Klypin, J. Kormendy, D. Lynden-Bell, F. Masset, I. Shlosman Ch. Skokos and M. Weinberg. I thank Jean-Charles Lambert for his invaluable help with the simulation software and the administration of the runs and W. Dehnen for making available to me his tree code and related programs. I also thank the Observatoire de Marseille, the region PACA, the INSU/CNRS and the University of Aix-Marseille I for funds to develop the computing facilities used for the calculations in this paper.

## References

Athanassoula, E., *Monthly Notices of the Royal Astronomical Society*, 259, 365, 1992.

Athanassoula, E. In R. Buta, D.A. Crocker and B.G. Elmegreen *Barred Galaxies*, pages 309, Astron. Soc. Pac. Conf. Series 91, 1996.

Athanassoula, E. *Astrophysical Journal Letters*, 569, L83, 2002 (A02).

Athanassoula, E. *Monthly Notices of the Royal Astronomical Society*, 341, 1179, 2003a (A03).

Athanassoula, E. In J. Makino and P. Hut, editors, *Astrophysical supercomputing using particles*, Astron. Soc. Pac. Conference Series, IAU Symp., 208, 177, 2003b.

Athanassoula, E. *Celestial Mechanics and Dynamical Astronomy*, 45, 9, 2005.

Athanassoula, E., Bienaymé, O., Martinet, L., Pfenniger, D. *Astronomy and Astrophysics* 127, 349, 1983.

Athanassoula, E., Bosma, A., Mujica, R. *Disks of Galaxies : Kinematics, Dynamics and Perturbations*, Astron. Soc. Pac. Conf. Series 275, 2002.

Athanassoula, E., Lambert, J. C., Dehnen, W. *Monthly Notices of the Royal Astronomical Society*, submitted, 2005.

Athanassoula, E., Misiriotis, A. *Monthly Notices of the Royal Astronomical Society*, 330, 35, 2002 (AM02).

Athanassoula, E., Morin, S., Wozniak, H., Puy, D., Pierce, M. J., Lombard, J., Bosma, A. *Monthly Notices of the Royal Astronomical Society*, 245, 130, 1990.

Athanassoula, E., Sellwood, J. A. *Monthly Notices of the Royal Astronomical Society*, 221, 213, 1986.

Berentzen, I., Athanassoula, E., Heller, C. H. ,Fricke, K. J. *Monthly Notices of the Royal Astronomical Society*, 347, 220, 2004.

Berentzen, I., Heller, C. H. Shlosman I. & Fricke, K. J. *Monthly Notices of the Royal Astronomical Society*, 300, 49, 1998.

Binney, J. *Monthly Notices of the Royal Astronomical Society*, 201, 1, 1982.

Binney, J., Gerhard, O., Hut, P. *Monthly Notices of the Royal Astronomical Society*, 215, 59, 1985.

Binney, J., Tremaine, S. *Galactic Dynamics*, Princeton Univ. Press, 1987.

Block, D., Freeman, K. C., Puerari, I., Groess, R., Block, L. *Penetrating bars through masks of cosmic dust: The Hubble Tuning Fork Strikes a New Note*, Kluwer publ., in press, 2005.

Bosma, A. In G. Longo, M. Capaccioli and G. Busarello *Morphological and Physical Classification of Galaxies*, p. 207, Kluwer pub., 1992.

Bottema, R. *Monthly Notices of the Royal Astronomical Society*, 344, 358, 2003.

Buta, R.J. *Astrophysical Journal Supplements*, 61, 609, 1986.

Buta, R., Crocker, D.A., Elmegreen, B.G. *Barred Galaxies*, Astron. Soc. Pac. Conf. Series 91, 1996.

Chandrasekhar, S. *Astrophysical Journal*, 97, 255, 1943.

Contopoulos, G. *Astronomy and Astrophysics*, 81, 198, 1980.

Contopoulos, G. *Order and chaos in Dynamical Astronomy*, Springer, 2002.

Contopoulos, G., Grosbøl, P. *Astronomy and Astrophysics Reviews*, 1, 261, 1989.

Contopoulos, G., Papayannopoulos, T. *Astronomy and Astrophysics*, 92, 33, 1980.

Debattista, V. P., Sellwood, J. A. *Astrophysical Journal*, 543, 704, 2000.

Efstathiou, G., Lake, G., Negroponte, J. *Monthly Notices of the Royal Astronomical Society*, 199, 1069, 1982.

Elmegreen, B.G., Elmegreen, D.M. *Astrophysical Journal*, 288, 438, 1985.

Elmegreen, D.M., Elmegreen, B.G., Bellin, A.D. *Astrophysical Journal*, 364, 415, 1990.

El-Zant, A., Shlosman, I. *Astrophysical Journal*, 577, 626, 2002.

El-Zant, A., Shlosman, I. *Astrophysical Journal*, 595, L41, 2003.

Eskridge et al. *Astronomical Journal*, 119, 536, 2000.

Ferrers, N. M. *Q. J. Pure Appl. Math.*, 14, 1, 1877.

Gadotti, D. A., de Souza, R. E. *Astrophysical Journal*, 583, L75, 2003.

Grosbøl P., Pompei, E., Patsis, P. A. In E. Athanassoula, A. Bosma and R. Mujica *Disks of galaxies : Kinematics, dynamics and perturbations*, 305, Astron. Soc. Pac. Conf. Series 275, 2002.

Hasan, H., Norman, C. *Astrophysical Journal*, 361, 69, 1990.

Hasan, H., Pfenniger, D., Norman, C. *Astrophysical Journal*, 409, 91, 1993.

Hernquist, L., Weinberg, M. *Astrophysical Journal*, 400, 80, 1992.

Hohl, F. *Astrophysical Journal*, 168, 343, 1971.

Holley-Bockelmann, K., Weinberg, M. D., Katz, N. *astro-ph/0306374*, 2003.

Hozumi, S., Hernquist, L. *astro-ph 9806002*, 1998.

Hozumi, S., Hernquist, L. In D. Merritt, J. A. Sellwood and M. Valluri, *Galaxy Dynamics*, Astron. Soc. Pac. Conf. Series 182, 259, 1999.

Hozumi, S., Hernquist, L. *Publications of the Astronomical Society of Japan*, submitted

2004.

Kalnajs, A. J. *Astrophysical Journal*, 166, 275, 1971.

Kandrup, H. E., Eckstein, B. L., Bradley, B. O. *Astronomy and Astrophysics*, 320, 65, 1997.

Kormendy, J. In L. Martinet and M. Mayor *Morphology and Dynamics of Galaxies*, Geneva Obs. publ., Geneva, 1982.

Little, B., Carlberg, R. G. *Monthly Notices of the Royal Astronomical Society*, 250, 161, 1991a.

Little, B., Carlberg, R. G. *Monthly Notices of the Royal Astronomical Society*, 251, 227, 1991b.

Lynden-Bell, D., Kalnajs, A. J. *Monthly Notices of the Royal Astronomical Society*, 157, 1, 1972.

Michalodimitrakis, M. *Astrophysics and Space Science*, 33, 421, 1975.

Miller, R. H., Prendergast, K. H., Quirk, W. J. *Astrophysical Journal*, 161, 903, 1970.

Norman, C., Sellwood, J. A., Hasan, H. *Astrophysical Journal*, 462, 114, 1996.

Ohta, K. In R. Buta, D. A. Crocker and B. G. Elmegreen *Barred Galaxies*, Astron. Soc. Pac. Conf. Series 91, 37, 1996.

Ohta, K., Hamabe, M., Wakamatsu, K. In R. Buta, D.A. Crocker and B.G. Elmegreen *Barred Galaxies*, Astron. Soc. Pac. Conf. Series 91, 37, 1990.

O'Neill, J. K., Dubinski, J. *Monthly Notices of the Royal Astronomical Society*, 346, 251, 2003.

Ostriker, J. P., Peebles, P. J. E. *Astrophysical Journal*, 186, 467, 1973.

Patsis, P. A., Athanassoula, E., Quillen, A. *Monthly Notices of the Royal Astronomical Society*, 483, 731, 1997.

Patsis, P. A., Skokos, Ch., Athanassoula, E. *Monthly Notices of the Royal Astronomical Society*, 337, 578, 2002.

Patsis, P. A., Skokos, Ch., Athanassoula, E. *Monthly Notices of the Royal Astronomical Society*, 342, 69, 2003.

Pfenniger, D. *Astronomy and Astrophysics*, 134, 373, 1984a.

Pfenniger, D. *Astronomy and Astrophysics*, 141, 171, 1984b.

Pfenniger D. Friedli D. *Astronomy and Astrophysics*, 252, 75, 1991.

Sandage, A. *The Hubble Atlas of Galaxies*, Carnegie Inst. Publ., Washington, 1961.

Shen, J., Sellwood, J. A. *Astrophysical Journal*, 604, 614, 2004.

Skokos, Ch., Patsis, P. A., Athanassoula, E. *Monthly Notices of the Royal Astronomical Society*, 333, 847, 2002a.

Skokos, Ch., Patsis, P. A., Athanassoula, E. *Monthly Notices of the Royal Astronomical Society*, 333, 861, 2002b.

Sparke, L. S. Sellwood, J. A. *Monthly Notices of the Royal Astronomical Society*, 225, 653, 1991.

Teuben, P. J., Sanders, R. H. *Monthly Notices of the Royal Astronomical Society*, 212, 257,

1985.

Toomre, A. *Annual Reviews of Astronomy & Astrophysics*, 15, 437, 1977.

Tremaine, S., Weinberg, M. D. *Monthly Notices of the Royal Astronomical Society*, 209, 729, 1984.

Valenzuela, O., Klypin, A. *Monthly Notices of the Royal Astronomical Society*, 345, 406, 2003.

de Vaucouleurs, G., Freeman, K. C. *Vistas in Astronomy*, 1, 163, 1972.

Weinberg, M. D. *Monthly Notices of the Royal Astronomical Society*, 213, 451, 1985.

Weinberg, M. D. *Monthly Notices of the Royal Astronomical Society*, astro-ph/0404169, 2004.